High performance phototransistors based on single crystalline perylene-tetracarboxylic-dianhydride nanoparticle

Linh-Nam Nguyen,[1,2,3] Sunil Kumar Pradhan,[1,2,3] Chia-Nan Yen,[4] Ming-Chou Lin,[1] Chien-Han Chen,[5] Cen-Shawn Wu,[5] Kuei-Shu Chang-Liao,[2] Minn-Tsong Lin,[4,6,a)] and Chii-Dong Chen[1,a)]

[1]*Institute of Physics, Academia Sinica, Taipei 115, Taiwan*
[2]*Department of Engineering and System Science, National Tsing Hua University, Hsinchu 300, Taiwan*
[3]*Nano Science and Technology Program, Taiwan International Graduate Program, Academia Sinica, Taipei 115, Taiwan*
[4]*Department of Physics, National Taiwan University, Taipei 106, Taiwan*
[5]*Department of Physics, National Chang-Hua University of Education, Chang-Hua 500, Taiwan*
[6]*Institute of Atomic and Molecular Sciences, Academia Sinica, Taipei 115, Taiwan*

(Received 20 August 2013; accepted 14 October 2013; published online 29 October 2013)

Organic semiconducting devices suffer from grain boundary scattering, which can be responsible for low mobility and even mask intrinsic transport properties. In this letter, we show that devices containing only single grains give electron mobility 2–3 orders higher than that of conventional film-structured polycrystalline organic semiconductor transistors. The devices contain single perylene-tetracarboxylic-dianhydride nanoparticles embedded inside gated-nanopore structures. Since there is no inter-grain scattering, we obtain the highest reported electron mobility values of 0.08 cm^2/Vs at 300 K and 0.5 cm^2/Vs at 80 K. Consequently, the devices, when illuminated with ultraviolet, also yield a previously unrecorded high value of external quantum efficiency of 3.5×10^6. © *2013 AIP Publishing LLC*. [http://dx.doi.org/10.1063/1.4827975]

Organic semiconductors have attracted broad interest in the fields of electronics and optoelectronics due to their low cost, high flexibility, light weight, and ease of processing. Possible applications for their use include active-matrix organic light-emitting-diode displays,[1] organic smart pixels,[2] organic solar cells,[3] and organic field-effect-transistors (OFETs).[4,5] However, most organic semiconductor devices suffer from low carrier mobility due to carrier scatterings caused by structural defects or grain boundaries. These problems occur in films with polycrystalline or amorphous structures. To reduce scattering in organic semiconductors, devices containing nano/micro-structured single crystals have been explored,[6–9] and high photo-sensitivity, photo-responsivity, and external quantum efficiency (EQE) were obtained. Among organic semiconductor materials, perylene tetracarboxylic dianhydride (PTCDA) is a promising candidate for electronic devices. The high temperature stability, significant intermolecular interactions between π-electrons and highly ordered structures on a wide variety of substrates make it significant for optoelectronic device applications, such as photoconductors,[10] organic photovoltaic cells,[11] organic light-emitting diodes,[12] and organic thin film transistors.[13] Besides, the study of absorption,[14] electro-absorption,[15] photoluminescence,[16] and photoconduction[17] in PTCDA further provides an important pathway understanding the fundamental optical processes in organic semiconductors. However, similar to all other organic materials, PTCDA films show low electron mobility values of approximately 10^{-5}–10^{-4} cm^2/Vs.[18] It was shown that in the absence of structural defects, large films containing single crystalline PTCDA exhibit one order of magnitude improvement in electron mobility;[19] however, the issue concerning grain boundary scattering is overlooked. Carrier scattering at grain boundaries inevitably limits the overall mobility of a film consisting of crystalline domains. In order to eliminate grain boundary scattering and explore the intrinsic mobility of PTCDA, single grain devices need to be examined. It is reported that crystalline PTCDA grains exist in two possible forms (α- and β-like structures) depending on their monoclinic unit cell parameters.[20,21] We propose that for small grains (i.e., nanoparticles) the entire particle should be of a single crystalline structure. This has been justified for other organic semiconducting materials even for grains of micrometer size.[22–24] Most importantly, electronic devices containing only a single nanoparticle may be of particular interest as they possess several advantages over their 1D and 2D counterparts. An obvious advantage is the large surface-to-volume ratio, which promises high sensitivity with light illumination. Another advantage is the short conduction channel length, which can facilitate short carrier transferring time. Thus, we expect devices containing only a single nanoparticle will exhibit extraordinary enhancements in carrier mobility, which will lead to promising possibilities for new electronic and/or opto-electronic applications. In this work, a PTCDA nanoparticle is embedded in a nanopore structure. The particle is surrounded by a gate electrode and sandwiched between an ultrathin aluminum oxide (Al_xO) insulator and aluminum (Al) electrodes at its top and bottom. Room temperature electron mobility is as high as 0.08 cm^2/Vs, about 1 order higher than previously recorded values for PTCDA single crystal films.[19] In view of the absence of grain boundary scattering, we think that this value is approaching the intrinsic electron mobility of PTCDA. Furthermore, the device shows an EQE value of 3.5×10^6, which is the highest reported value so far

a)Electronic addresses: chiidong@phys.sinica.edu.tw and mtlin@phys.ntu.edu.tw

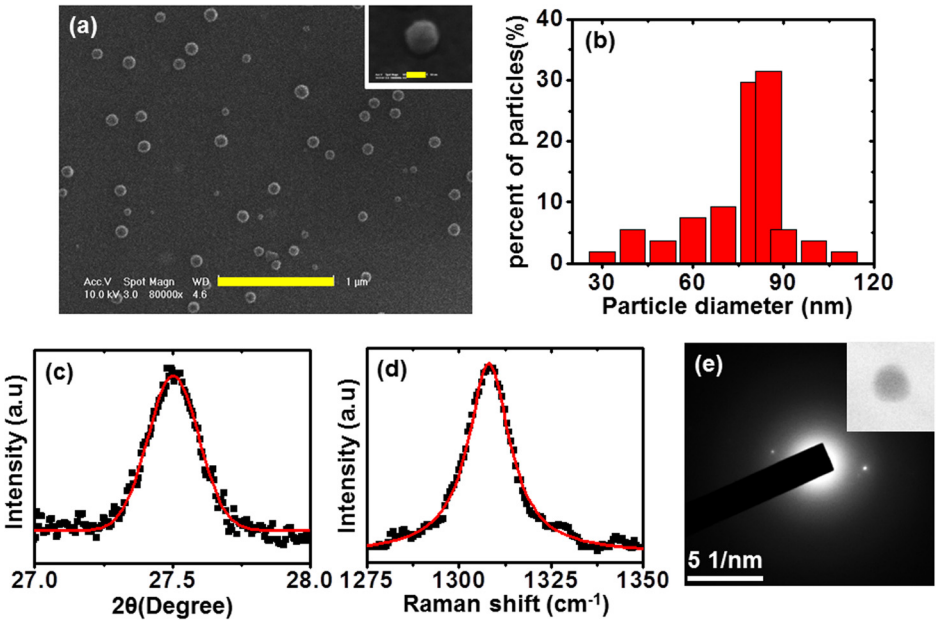

FIG. 1. Characterizations of PTCDA nanoparticles on a Si_3N_4 membrane. (a) SEM image. The scale bar is 1 μm. The inset shows tilt-angle view of a single nanoparticle. The scale bar is 50 nm. (b) Particle size distribution of the nanoparticles. Most of particles have diameters about 80–85 nm. (c) The (102) X-ray diffraction peak. (d) Raman spectrum of δ_{C-H} mode of PTCDA nanoparticles. In (c) and (d), black squares are experimental data and the red curves are fitting curves. (e) The SAED pattern of a single PTCDA nanoparticle.

for opto-electronic devices made of organic single crystals. Mechanisms governing gate modulation and photo-induced electron transport are discussed.

PTCDA powder (purity 97%, Sigma-Aldrich) was thermally deposited onto 30 nm-thick silicon nitride (Si_3N_4) membranes in a vacuum chamber with a base pressure of 2.5×10^{-8}millibars. During evaporation, the substrate was maintained at 27 °C, and the crucible temperature was kept at around 420 °C, giving a deposition rate of ~1 Å/s. Fig. 1(a) shows that after vaporization of nominally 20 nm-thick PTCDA on the Si_3N_4 membrane, well-separated spherical PTCDA nanoparticles were formed. Based on scanning electron microscope (SEM) inspections, the particle diameter determined from particle distribution (Fig. 1(b)) was about 80–85 nm. The crystalline properties of these nanoparticles were characterized by using X-ray diffraction (XRD), Raman spectroscopy, and Transmission electron microscopy (TEM). The XRD (with source: Cu Kα, $\lambda = 1.5415$ Å) spectrum shown in Fig. 1(c) displays a single diffraction peak around $2\theta = 27.5°$, corresponding to diffraction from the (102) plane of the β-phase structure of single crystal PTCDA.[25] The single Gaussian peak has a full width at half maxima (FWHM) of 0.218°. In accordance with the Scherrer's formula, this FWHM implies a particle size of 75 nm. The β-phase PTCDA crystal is reconfirmed by Raman spectrum measurement with a light source of 532 nm. Fig. 1(d) shows the spectral region of the most prominent internal mode contribution from C-H bending in PTCDA. A Lorentzian fitting indicates a peak value of 1308.1 cm^{-1}, which is a signature of β-PTCDA phase crystal structure.[25,26] As a comparison, in

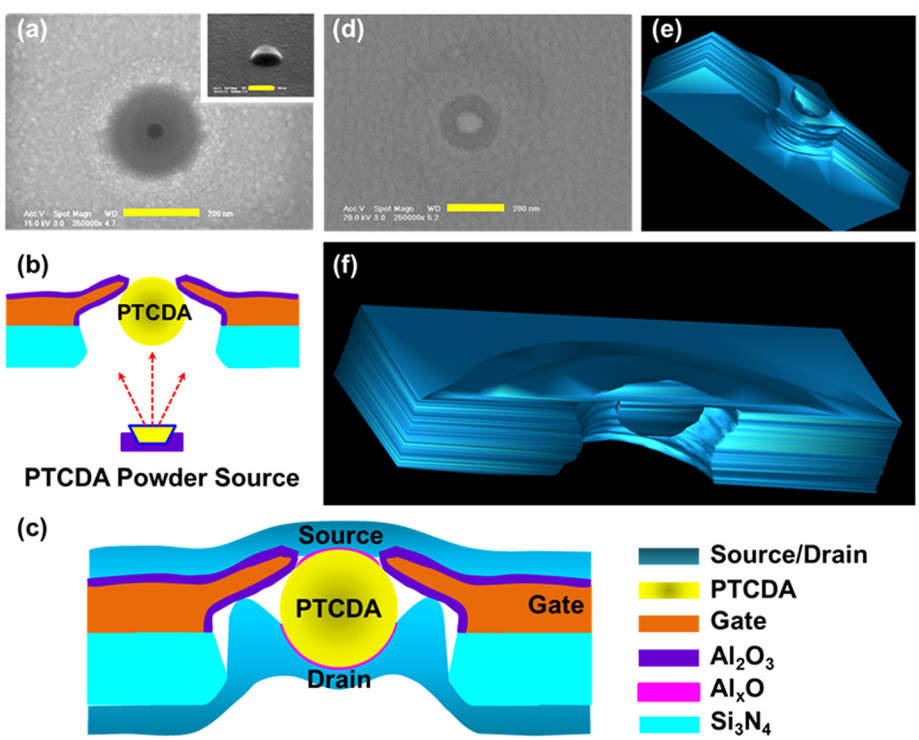

FIG. 2. (a) SEM images of top view (main panel) and tilt-angle view (the inset) of a nanopore with a metal gate. The scale bar is 200 nm. (b) Thermal deposition of PTCDA nanoparticle on the bottom side of nanopore. (c) A cross-sectional schematic illustration of the nanopore device with a gated single PTCDA nanoparticle that is sandwiched between Al_xO/Al source and drain electrodes. (d) SEM image showing a deposited single PTCDA nanoparticle located in the bottom side of a nanopore. The scale bar is 200 nm. (e) and (f) Reconstructed 3D-TEM images of bottom view and cross-sectional view of the nanoparticle embedded inside nanopore. The 3D-TEM images are reconstructed from 61 images taken from +30° to -30° with a tilt increment of 1° on a Linux workstation using the IMOD software. Individual projection images of the tilt series are aligned with cross-correlation; the tomographic reconstruction is calculated by weighted back-projection (see Ref. 28).

α-phase PTCDA single crystal the Raman peak of C-H bending appears at 1302 cm^{-1}.[27] Finally, the selected area electron diffraction (SAED) pattern of a single nanoparticle, as shown in Fig. 1(e), also clearly indicates highly crystalline structure of the nanoparticles deposited on Si_3N_4 membranes.

The device structure and fabrication process are illustrated in Fig. 2. Electron-beam lithography and reactive ion-etching were employed to create a bowl-shaped pore on a 30 nm-thick silicon nitride (Si_3N_4) membrane. Details of nanopore fabrication procedure can be found in Ref. 28. The pore was surrounded by a volcano-shaped gate electrode made of 18 nm-thick Al. The gate electrode was covered by an 8 nm-thick Al_2O_3 layer, which served as an insulating layer to prevent possible leakage to the top and bottom electrodes (to be made at a latter stage). The volcano structure on the membrane had a pore on the top with a diameter of about 44 nm, as shown in the SEM images in Fig. 2(a). After fabrication of nanopores, PTCDA nanoparticles were thermally deposited on the bottom side of the nanopores, as illustrated in Fig. 2(b). This deposition process was then followed by coating of ultrathin Al_xO blocking layers onto both sides of the nanoparticle by oxidation of 0.6 nm-thick RF-sputtered Al layers using oxygen plasma. Subsequently, 30nm-thick Al top/bottom electrodes (Source/Drain) were DC-sputtered onto the blocking layers. The Al_xO interface blocking layer was to prevent Al from diffusing into PTCDA and was crucial for the device's performance. The completed device structure is schematically illustrated in Fig. 2(c). The surrounding gate structure yielded strong capacitive coupling to the nanoparticle.

To investigate in detail, the nanoparticle structure inside the nanopore, we made a TEM inspection of the nanoparticle using 3D-TEM tomography technique. In Fig. 2(d), we show an SEM image of a PTCDA particle located inside the pore, which can be seen clearly in the reconstructed 3D-TEM images displayed in Figs. 2(e) and 2(f). From these images, diameter of the particle is found to be about 80 nm, also the opening of Si_3N_4 pore is about 200 nm and the pore edge profile is roughly of S-shape. The particle is well-separated from the pore edge and its top is attached to the Al_2O_3 surface on the bottom side of the Al-gate electrode. 25 devices were made in this work, but only about 8% of devices showed gate voltage (V_g) modulation of current-drain voltage (I-V_{ds}) curves, i.e., output characteristics. Failed devices that contained no nanoparticle normally exhibited resistances ranging between a few tens to ~1 kΩ, and no gate modulation. This is attributed to the contact resistance between top and bottom Al electrodes with an uncontrolled contact area. The contact resistance decreased with decreasing temperature, which is a sign of metal contact. Contrarily, we show below that the devices with embedded nanoparticles display strikingly different behaviors such as high resistance (about 100 kΩ–1 MΩ), prominent gate modulation and increased device resistance upon cooling.

In this paper, we present data from two devices, which are denoted as devices A and B. Fig. 3(a) shows gate voltage modulation of current-drain voltage curves; the inset displays differential conductance $G \equiv dI/dV_{ds}$ as a function of V_g for device A at 80 K. The measured data for the two devices at 300 K are also shown in Fig. 3(b). The suppression of

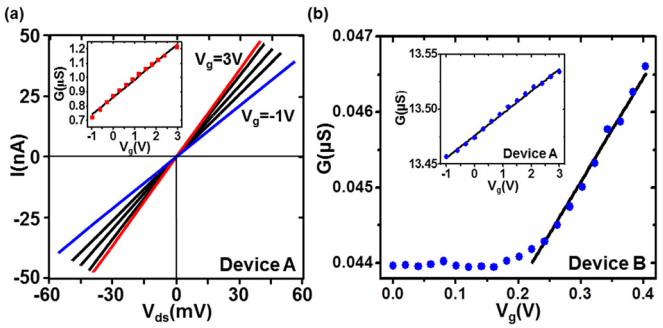

FIG. 3. (a) I-V_{ds} characteristics for device A at 80 K for gate voltages varying from −1 V (blue) to 3 V (red) with a step size of 1 V. The inset shows gate dependence of differential conductance dI/dV_{ds} at $V_{ds} = 20$ mV (red squares). The black line is a linear fit to the data, giving $dG/dV_g = 0.124$ μS/V. (b) Gate modulation of differential conductance (blue circles) at 300 K for devices A (inset) and B (main panel). The fits (black lines) yield dG/dV_g values of 0.02 μS/V and 0.014 μS/V for device A and device B, respectively.

current at negative gate voltages (data range not shown here) indicates that the PTCDA nanoparticle is of n-type. The gate dependence of differential conductance is almost linear and is depicted in Figs. 3(a) and 3(b). In this linear operation regime, electron mobility is independent of V_{ds} and can be evaluated using the following relation:

$$\mu = \frac{dG}{dV_g}\frac{L^2}{C_g}, \tag{1}$$

where L is the effective channel length. As argued in the supporting information, this length is roughly $\sqrt{2}R$, where $R \approx 40$ nm is the particle radius. To determine gate capacitance C_g, the effective gate area is estimated in accordance with the illustration in Fig. S1.[29] Although an accurate estimate of the contact area, and hence gate capacitance, is not possible, if we assume that the contact angle is 7–10° (corresponding to a tangential arc between 5–7 nm) and oxide thickness is 6–8 nm, C_g can be estimated to be 8–15 aF (see supplementary material[29] for detailed calculations). Accordingly, we obtained an electron mobility value of 0.045–0.08 cm^2/Vs at 300 K. Using the same approach, the mobility at room temperature for device B is determined to be 0.03–0.055 cm^2/Vs. This value is 1 order in magnitude greater than the best reported value for single crystals[19] and 2–3 orders higher than those reported for polycrystalline films.[18] The high electron mobility values in our PTCDA device can be attributed to: (1) the elimination of grain boundary scattering because the nanoparticle is of single domain and (2) the prevention of hybrid layer through the use of Al_xO.[30,31] The hybrid layer is formed from the reaction between Al and anhydride (C-O) end group in PTCDA.[32]

Temperature dependence of mobility is studied and displayed in Fig. 4(a). Upon cooling, mobility first increases and then decreases. At around 80 K, which we refer to as T_{cr}, the mobility reaches a maximum value of 0.5 cm^2/Vs. T_{cr} is the crossover temperature that separates high-temperature electron-phonon scattering from low-temperature Coulomb scattering mechanisms. The initial increase (at $T > T_{cr}$) is from suppression of electron-phonon scattering, which is a manifestation of a band-like transport mechanism.[33,34] In organic

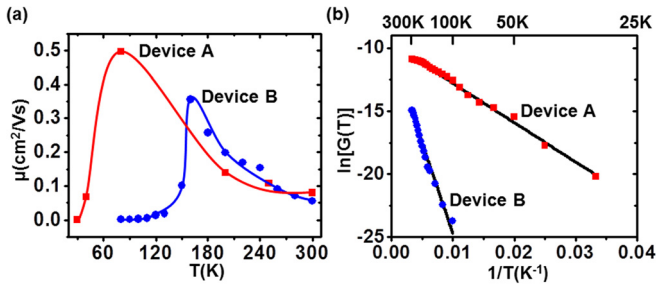

FIG. 4. (a) Temperature dependence of electron mobility for devices A and B. T_{cr}, at which the maximum mobility appears, is around 80 K for device A and around 160 K for device B. (b) An Arrhenius plot showing temperature dependence of device conductance for devices A and B. Lines of best fit (black lines) yield activation energies of 27 meV and 124 meV for A and B, respectively.

semiconductor materials, band-like transport can only be observed in very pure organic single crystals.[35,36] Below T_{cr}, the mobility decreases dramatically and drops to about 10^{-4} cm^2/Vs at 30 K. But we note that at this temperature range the carrier concentration also decreases significantly as evidenced by the decrease in conductance with decreasing temperature in Fig. 4(b). Because of the decreased carrier concentration, the screening effect is weakened, promoting Coulomb interaction between carriers, and reducing the carrier mobility. In addition, the impurity scattering gains importance at low temperatures and is also responsible for the reduced mobility.[35,37,38] Although similar mobility temperature dependence is observed for device B, the T_{cr} appears at around 160 K, which is clearly higher than that of device A. This may be explained by carrier concentration in device B being lower than A, as indicated by the comparison between the activation energies in Fig. 4(b). The difference in the carrier concentration may probably be attributed to unintentional and uncontrolled contaminations during the evaporations of PTCDA and/or Al_xO. The low carrier concentration in device B results in strong electric-field screening, which, in turn, yields a higher T_{cr}. Similar dependence of T_{cr} on carrier concentration for organic single crystal was reported.[39]

To explore the effects of high mobility on opto-electronic properties, the photo-response of devices is investigated. Illumination with photon energy above the energy bandgap of PTCDA excites excess carriers and enhances electric conduction. Here, the device is illuminated on the top side by an ultraviolet light emitting diode (UV-LED) with photon energy ~3.0 eV (wavelength ≈ 405 nm) higher than the bandgap of PTCDA (2.2 eV).[18,40] Fig. 5(a) shows dependence of device conductance and electron mobility on UV-light intensity. Interestingly, while conductance increases with light intensity, mobility decreases. This may be due to additional scattering by increased photon-induced excess carriers.

EQE,[9,41,42] defined as the number of exited carriers induced by an incident photon and per unit time, can be determined by using the following equation:

$$EQE = \frac{I_{ph}}{P_{ill}} \times \frac{hc}{\lambda e}, \tag{2}$$

where I_{ph} is the photo-induced current and P_{ill} is incident illumination power on the particle through the nanopore window. h, e, c, and λ are Planck's constant, electron charge, speed of light, and incident light wavelength, respectively. Fig. 5(b) shows light intensity dependence of photocurrent and EQE values. It is found that EQE is as high as 3.5×10^6 for a light intensity of 0.12 mW/cm^2, which is 2–3 orders in magnitude higher than previously reported values for organic semiconductors, such as single crystalline Ribbons (1.3×10^3)[6] and single N,N′-bis(2-phenylethyl)-perylene–3,4:9,10-tetracarboxylic diimide (BPE-PTCDI) nanowires $(2.6 \times 10^5\%)$.[9] Furthermore, the obtained value is comparable to those of nano-structured inorganic semiconductors such as $In_2Ge_2O_7$ nanobelts (3.5×10^6)[41] and SnO_2 nanowires (1.3×10^7).[42] The high EQE can be attributed[9,41,42] to large active surface area, short travelling distance and the intrinsically defect-free nature of single crystalline. The former two are due to nanoparticle geometry and the latter two help to reduce the recombination probability. It is also noted that EQE decreases with increasing light intensity. Similar behavior has been reported previously[8,9] and attributed to the reduced electron mobility with increasing illumination power. The results of this study are in keeping with electron mobility's dependence on luminescence intensity.

Fig. 5(c) presents the results of the device's photo-response time. It shows that photo-response switching behavior is stable, and decay time is independent of light intensity. The latter is obtained by fitting photocurrent response to a double exponential decay function in Fig. 5(d). The fast and slow decay behaviors can be attributed to carrier relaxations via interband and interface state excitations, respectively.[43] However, we note that the decay time of these photo carriers is short compared to those of PTCDA thin-film literature reports,[43] implying fewer defects available for charge

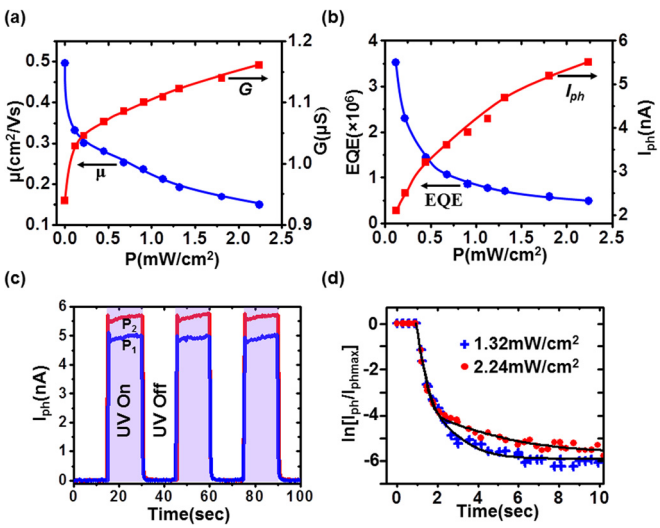

FIG. 5. (a) Illumination intensity dependence of electron mobility (blue circles) and conductance (red squares); (b) Illumination intensity dependence of external quantum efficiency (blue circles) and photocurrent (red squares). Note: With increasing intensity, both conductance and photocurrent increase but mobility and EQE decrease; (c) time dependence of photocurrent with different UV intensities: $P_1 = 1.32$ mW/cm^2 (blue curve), $P_2 = 2.24$ mW/cm^2 (red curve); and (d) double exponential fittings of photocurrent decay curves. Experimental data are presented for UV intensities of 1.32 mW/cm^2 (blue crosses) and 2.24 mW/cm^2 (red dots). The fast time constant for the two intensities is 0.18 s, whereas the slow time constants for them are 1.9 s and 2.3 s, respectively. All measurements shown here are performed at 80 K.

trapping. This suggests an absence of domain boundary scattering and explains the high mobility values obtained. This is further supported by crystalline organic semiconductors having a fast response time compared to polycrystalline films; for example, naphthalene tetracarboxylic dianhydride (NTCDA)[44] and other organic materials.[7–9,45]

In conclusion, we show that the electron mobility of PTCDA nanoparticles can be very high as 0.08 cm^2/Vs at 300 K and 0.5 cm^2/Vs at 80 K. These values may be approaching the intrinsic electron mobility of PTCDA. Temperature dependence of mobility peaks in line with previously reported peaking mechanisms for single crystal organic semiconductors. With such high mobility, the device also shows a fast response time. Its recorded high EQE value was 3.5×10^6. A single nanoparticle device eliminates the deleterious effects of defects and grain-boundary recombination. It also facilitates fast transfer times due to short travel distances. These characteristics greatly increase possible applications of organic semiconductors in electronic and opto-electronic devices.

We thank Tzu-Hui Hsu and Teik-Hui Lee for their assistance during the course of this work. This research was funded by the National Science Council of Taiwan under Contract Nos. NSC 101-2112-M-001-028-MY3 and NSC 100-2120-M-002-002. Technical support from NanoCore, the Core Facilities for Nanoscience and Nanotechnology at Academia Sinica, is acknowledged.

[1]S. H. Ju, J. F. Li, J. Liu, P. C. Chen, Y. G. Ha, F. Ishikawa, H. K. Chang, C. W. Zhou, A. Facchetti, D. B. Janes, and T. J. Marks, Nano Lett. **8**, 997–1004 (2008).
[2]A. Dodabalapur, Z. Bao, A. Makhija, J. G. Laquindanum, V. R. Raju, Y. Feng, H. E. Katz, and J. Rogers, Appl. Phys. Lett. **73**, 142 (1998).
[3]D. Wohrle and D. Meissner, Adv. Mater. **3**, 129–138 (1991).
[4]G. Horowitz, Adv. Mater. **10**, 365–377 (1998).
[5]C. D. Dimitrakopoulos and P. R. L. Malenfant, Adv. Mater. **14**, 99–117 (2002).
[6]Y. Guo, C. Du, G. Yu, C. Di, S. Jiang, H. Xi, J. Zheng, S. Yan, C. Yu, W. Hu, and Y. Liu, Adv. Funct. Mater. **20**, 1019–1024 (2010).
[7]K. H. Kim, S. Y. Bae, Y. S. Kim, J. A. Hur, M. H. Hoang, T. W. Lee, M. J. Cho, Y. Kim, M. Kim, J. Jin, S. Kim, K. Lee, S. J. Lee, and D. H. Choi, Adv. Mater. **23**, 3095–3099 (2011).
[8]Y. Zhou, L. Wang, J. Wang, J. Pei, and Y. Cao, Adv. Mater. **20**, 3745–3749 (2008).
[9]H. Yu, Z. Bao, and J. H. Oh, Adv. Funct. Mater. **23**, 629–639 (2013).
[10]K. Y. Law, Chem. Rev. **93**, 449 (1993).
[11]C. W. Tang, Appl. Phys. Lett. **48**, 183 (1986).
[12]Z. Shen, P. E. Burrows, V. Bulović, S. R. Forrest, and M. E. Thompson, Science **276**, 2009–2011 (1997).
[13]S. Kowarik, A. Gerlach, and F. Schreiber, J. Phys. Condens. Matter **20**, 184005 (2008).
[14]V. Bulović and S. R. Forrest, Chem. Phys. **210**, 13–25 (1996).
[15]Z. Shen, P. E. Burrows, S. R. Forrest, M. Ziari, and W. H. Steier, Chem. Phys. Lett. **236**, 129–134 (1995).
[16]A. Y. Kobitski, R. Scholz, D. R. T. Zahn, and H. P. Wagner, Phys. Rev. B **68**, 155201 (2003).
[17]V. Bulović and S. R. Forrest, Chem. Phys. Lett. **238**, 88–92 (1995).
[18]J. R. Ostrick, A. Dodabalapur, L. Torsi, A. J. Lovinger, E. W. Kwock, T. M. Miller, M. Galvin, M. Berggren, and H. E. Katz, J. Appl. Phys. **81**, 6804 (1997).
[19]K. Yamada, J. Takeya, T. Takenobu, and Y. Iwasa, Appl. Phys. Lett. **92**, 253311 (2008).
[20]B. Krause, A. C. Dürr, K. Ritley, F. Schreiber, H. Dosch, and D. Smilgies, Phys. Rev. B **66**, 235404 (2002).
[21]K. Akers, R. Areca, A. Hor, and R. O. Loutfy, J. Phys. Chem. **91**, 2954 (1987).
[22]A. L. Briseno, S. C. B. Mannsfeld, M. M. Ling, S. Liu, R. J. Tseng, C. Reese, M. E. Roberts, Y. Yang, F. Wudl, and Z. Bao, Nature **444**, 913 (2006).
[23]A. Lv, S. R. Puniredd, J. Zhang, Z. Li, H. Zhu, W. Jiang, H. Dong, Y. He, L. Jiang, Y. Li, W. Pisula, Q. Meng, W. Hu, and Z. Wang, Adv. Mater. **24**, 2626–2630 (2012).
[24]L. Jiang, W. Hu, Z. Wei, W. Xu, and H. Meng, Adv. Mater. **21**, 3649–3653 (2009).
[25]A. Das, G. Salvan, T. U. Kampen, W. Hoyer, and D. R. T. Zahn, Appl. Surf. Sci. **212–213**, 433–437 (2003).
[26]G. Salvan, D. A. Tenne, A. Das, T. U. Kampen, and D. R. T. Zahn, Org. Electron. **1**, 49–56 (2000).
[27]D. A. Tenne, S. Park, T. U. Kampen, A. Das, R. Scholz, and D. R. T. Zahn, Phys. Rev. B **61**, 14564 (2000).
[28]L. N. Nguyen, M. C. Lin, H. S. Chen, Y. W. Lan, C. S. Wu, K. S. Chang-Liao, and C. D. Chen, Nanotechnology **23**, 165201 (2012).
[29]See supplementary material at http://dx.doi.org/10.1063/1.4827975 for gate capacitance calculation.
[30]K. S. Li, Y. M. Chang, S. Agilan, J. Y. Hong, J. C. Tai, W. C. Chiang, K. Fukutani, P. A. Dowben, and M. T. Lin, Phys. Rev. B **83**, 172404 (2011).
[31]T. S. Santos, J. S. Lee, P. Migdal, I. C. Lekshmi, B. Satpati, and J. S. Moodera, Phys. Rev. Lett. **98**, 016601 (2007).
[32]Y. Hirose, A. Kahn, V. Aristov, P. Soukiassian, V. Bulovic, and S. R. Forrest, Phys. Rev. B **54**, 13748 (1996).
[33]O. D. Jurchescu, J. Baas, and T. T. M. Palstra, Appl. Phys. Lett. **84**, 3061 (2004).
[34]K. Nakayama, Y. Hirose, J. Soeda, M. Yoshizumi, T. Uemura, M. Uno, W. Li, M. J. Kang, M. Yamagishi, Y. Okada, E. Miyazaki, Y. Nakazawa, A. Nakao, K. Takimiya, and J. Takeya, Adv. Mater. **23**, 1626–1629 (2011).
[35]N. Karl, K. H. Kraft, J. Marktanner, M. Münch, F. Schatz, R. Stehle, and H. M. Uhde, J. Vac. Sci. Technol. A **17**, 2318–2328 (1999).
[36]C. Liu, T. Minari, X. Lu, A. Kumatani, K. Takimiya, and K. Tsukagoshi, Adv. Mater. **23**, 523–526 (2011).
[37]T. Ando, A. B. Fowler, and F. Stern, Rev. Mod. Phys. **54**, 437 (1982).
[38]M. H. Somerville, D. F. L. Greenberg, and J. A. D. Alamo, Appl. Phys. Lett. **64**, 3276 (1994).
[39]I. G. Lezama, M. Nakano, N. A. Minder, Z. Chen, F. V. Di Girolamo, A. Facchetti, and A. F. Morpurgo, Nature Mater. **11**, 788 (2012).
[40]J. Xue and S. R. Forrest, Phys. Rev. B **69**, 245322 (2004).
[41]W. Tian, C. Zhi, T. Zhai, X. Wang, M. Liao, S. Li, S. Chen, D. Golberg, and Y. Bando, Nanoscale **4**, 6318–6324 (2012).
[42]L. Hu, J. Yan, M. Liao, L. Wu, and X. Fang, Small **7**, 1012–1017 (2011).
[43]A. S. Komolov, E. F. Lazneva, S. A. Komolov, I. S. Busin, and M. V. Zimina, Semiconductors **45**, 169–173 (2011).
[44]M. Hiramoto, A. Miki, M. Yoshida, and M. Yokoyama, Appl. Phys. Lett. **81**, 1500 (2002).
[45]Q. Tang, L. Li, Y. Song, Y. Liu, H. Li, W. Xu, Y. Liu, W. Hu, and D. Zhu, Adv. Mater. **19**, 2624–2628 (2007).